# Preparation of Fe$_3$O$_4$/polysulfone ultrafiltration membrane and its adsorption of phosphate from aqueous solution

Bin Zhao[a,b], Xiuxiu Huang[b], Xiaona Wu[a,c], Liang Wang[a,*], Anqi Liu[b], Zhaohui Zhang[a,b], Junjing Li[a,b], Zijun Yu[b], Tengyao Xu[b]

[a]*State Key Laboratory of Separation Membranes and Membrane Processes, Tianjin Polytechnic University, Tianjin 300387, China,*
*email: zhaobin@tjpu.edu.cn (B. Zhao), wwxxnn218@126.com (X. Wu), Tel./Fax +86 22 83955163,*
*email: mashi7822@163.com (L. Wang), zzh7448@126.com (Z. Zhang), junjingli85@163.com (J. Li)*
[b]*School of Environmental and Chemical Engineering, Tianjin Polytechnic University, Tianjin 300387, China,*
*email: xiuxiuhuang15@126.com (X. Huang), liuanqi87627@163.om (A. Liu), 745773273@qq.com (Z. Yu),*
*1012150969@qq.com (T. Xu)*
[c]*School of Environmental Science and Engineering, Tianjin University, Tianjin 300072, China*

**ABSTRACT**

The fabrication of mixed matrix membranes (MMMs) is a promising method to improve the properties of polymer membrane. In this study, composite polysulfone (PSf) membrane was prepared by blending Fe$_3$O$_4$ nanoparticles (NPs) via non-solvent induced phase separation (NIPS) method. The as-prepared Fe$_3$O$_4$/PSf membranes with different Fe$_3$O$_4$ loadings (60% and 120%) were characterized using X-ray diffraction (XRD) and scanning electron microscopy (SEM). The membrane porosity, pore size, water flux, water contact angle, and bovine serum albumin (BSA) rejection were also analyzed. The presence of Fe$_3$O$_4$ NPs accelerated the phase inversion kinetics;therefore, membranes with opener finger-like structure and higher porosity were obtained. The Fe$_3$O$_4$/PSf membranes also demonstrated remarkable fouling resistance. When a 0.3 g·L$^{-1}$ BSA solution was used as feed, the stable flux after 2 h filtration markedly increased by over 20 times compared to the pristine PSf membrane. Batch adsorption tests indicated that the composite membranes can effectively remove phosphate at pH ranging from 4 to 8. The adsorption kinetics can be fitted by both pseudo-first order and pseudo-second order models with correlation coefficients higher than 0.96. Intra-particle diffusion was not the rate-limiting step in the whole adsorption process. The maximum adsorption capacity obtained by Langmuir isotherm was 0.684 mg-P·g$^{-1}$ for 120% Fe$_3$O$_4$/PSf membrane. In addition, the phosphate adsorption capability of the proposed Fe$_3$O$_4$/PSf membrane can be well recovered after regeneration using a 0.01 mol·L$^{-1}$ NaOH solution.

*Keywords:* Fe$_3$O$_4$ nanoparticles; Mixed matrix membrane; Ultrafiltration; Phosphate; Adsorption

## 1. Introduction

Excess discharge of wastewater rich in phosphorus to surface water is a crucial factor for water eutrophication, which poses a great threat to the safety of aquatic ecosystem and human health. The threshold value of total phosphorus (TP) for eutrophication is suggested to be less than 0.035 mg-P·L$^{-1}$ [1]. Enhanced removal of phosphorus from the effluent of wastewater treatment plant (WWTP) is thus important before its discharge into the environment. Conventional technologies for phosphorus removal include biological method, chemical precipitation, crystallization, adsorption and membrane filtration [2].

Among all the above technologies, adsorption is widely used due to its high efficiency, low energy consumption,

---

*Corresponding author.

and flexible operation [3]. Moreover, the exhausted adsorbent can be regenerated and used repeatedly; therefore, the additional cost was low. Various absorbents have been developed for phosphorus removal from aqueous solution, such as nanoparticles (NPs) containing iron oxides [4–6], aluminum oxides [7] as well as titanium oxides [8]. Since the electrostatic attraction and the formation of inner-sphere complexes are supported to be the main mechanisms, the overall phosphorus adsorption with these metal oxides is highly selective and stable. Even though NPs generally demonstrate fast adsorption kinetics and high adsorption capacity [9], the agglomeration and recovery of these small particles pose great problems in their practical applications [10]. As a result, many studies focus on loading these active materials on microspheres or fibers, or preparing magnetic adsorbent [11,12].

Membrane is a promising technology for both drinking water and wastewater treatment. It has been widely acclaimed for its high efficiency, high effluent quality, and high stability. Low pressure membrane processes, such as microfiltration (MF) and ultrafiltration (UF), generally function based on the size exclusion of the membrane pores. They can successfully retain particles and colloids and reduce the water turbidity, but barely remove dissolved pollutants with size smaller than pores, such as heavy metal cations and hazardous anions. Mixed matrix membranes (MMMs) is a kind of membrane incorporating organic fillers into the polymer matrices during the membrane fabrication [13]. The addition of inorganic NPs does not only improve the membrane properties in terms of high permeate flux and strong physical and chemical stability, but also gives membrane extra functions [14]. By introducing nano-adsorbent into membrane matrix, the removal of pollutants with small size can be accomplished at the same time of filtration for low pressure membrane processes. A hydrous ferric oxide (HFO)/polysulfone (PSf) composite membrane was prepared for Pb(II) removal from aqueous solution [12]. When the initial Pb(II) concentration was 35 mg·L$^{-1}$, the maximum adsorption capacity of the prepared membrane was 13.2 mg-Pb·g$^{-1}$. Effective desorption can be achieved using a 0.5 mol·L$^{-1}$ NaOH solution. PSf hollow fiber membrane embedded with Zr-based NPs was developed for arsenic removal, and its adsorption capacity was 131.8 mg-As·g$^{-1}$ [3]. Polyethersulfone (PES) membrane incorporating $Fe_3O_4$ NPs showed high affinity towards copper cation in solution [15]. These MMMs combine the adsorption capability together with the removal of suspended solids, bacteria, and natural organic matters, and no additional device for adsorbent separation is required any more. Therefore, the overall integrity of the water treatment system can be significantly improved.

In this study, a novel composite membrane ($Fe_3O_4$/PSf) was prepared by incorporating $Fe_3O_4$ NPs into PSf membrane. $Fe_3O_4$ NPs were synthesized by co-precipitation and the effects of $Fe_3O_4$ NPs loading on membrane morphology, overall porosity, pore size, and hydrophilicity were systematically investigated. The permeate flux was tested using deionized (DI) water and a bovine serum albumin (BSA) solution, respectively. The adsorption of phosphate by the $Fe_3O_4$/PSf membrane was studied in terms of kinetics and isotherm, and its regeneration and reusability were also evaluated.

## 2. Materials and methods

### 2.1. Materials

PSf (Udel P-3500) was supplied by Solvay, USA. 1-methyl-2-pyrrolidone (NMP, >99.5%) and polyethylene glycol 400 (PEG-400, >99.5%) were purchased from Tianjin Guangfu Chemical Co., China. BSA was purchased from Aladdin, China. Ferric chloride hexahydrate (FeCl$_3$·6H$_2$O), ferrous sulfatehexahydrate (FeSO$_4$·6H$_2$O), ammonia solution, potassium dihydrogen phosphate (KH$_2$PO$_4$), sodium chloride (NaCl), sodium sulfate (Na$_2$SO$_4$), and sodium bicarbonate (NaHCO$_3$) were supplied by Tianjin Kemiou Chemical Co., China.

### 2.2. Synthesis of $Fe_3O_4$ NPs

$Fe_3O_4$ NPs were prepared by co-precipitation according to the reported procedure [11]. FeCl$_3$·6H$_2$O (11.35 g) and FeSO$_4$·6H$_2$O (5.84 g) were dissolved in DI water (150 ml). The mixture was heated up to 60°C. Ammonia solution (25%, 40 ml) was then added under vigorous stirring. The solution was kept at 85°C for 30 min. After cooling to room temperature, the brownish suspended particles were collected using a magnet and washed several times with DI water. Finally, the as-obtained particles were dried at 40°C and grounded before use.

### 2.3. Fabrication of $Fe_3O_4$/PSf membranes

Non-solvent induced phase separation (NIPS) method was used to prepare $Fe_3O_4$/PSf membrane. The prepared $Fe_3O_4$ NPs were dispersed in NMP (66.3 ml), and the NPs loadings were 60% and 120% (relative to the polymer mass), respectively. After ultrasonic dispersion of the above solution for 30 min, PSf (17 g) and PEG-400 (12.9 ml) were added and stirred until complete dissolution. The dope was degassed overnight at room temperature, and then casted on a smooth glass plate using a glass rod. The casting film was subsequently immersed in a tap water bath. The prepared membrane was finally detached and transferred into fresh tap water to remove the residual solvent.

### 2.4. Filtration test

The permeate flux of the fabricated $Fe_3O_4$/PSf membrane was measured using a cross-flow UF cell. Membrane with an effective area of 3.86 × 10$^{-4}$ m$^2$ was equipped in the cell. Before the test, membrane was pre-compacted using DI water at 0.2 MPa for 30 min. Filtration was then carried out using DI water at 0.1 MPa. The permeate was collected and weighed by an online electronic balance. The flux was calculated using Eq. (1),

$$J = \frac{\Delta m_p}{\rho \cdot A \cdot \Delta t} \tag{1}$$

where $J$ (L·m$^{-2}$·h$^{-1}$) is the permeate flux; $\Delta t$ (h) is the sampling time interval; $\Delta m_p$ (kg) is the mass difference of the permeate during $\Delta t$; $\rho$ (kg·L$^{-1}$) is the density of the permeate; $A$ (m$^2$) is the effective membrane area.

A BSA solution of 0.3 g·L$^{-1}$ was used as the feed solution to evaluate the membrane separation capability as well as

its antifouling capability. The solution was prepared using a phosphate buffer solution of pH 7.4. The filtration lasted for 2 h for each membrane, and the time profile of the permeate flux was recorded. The BSA rejection efficiency ($R$, %) at 20th min was determined using Eq. (2),

$$R = \frac{C_0 - C_{20}}{C_0} \times 100\% \tag{2}$$

where $C_0$ (g·L$^{-1}$) and $C_{20}$ (g·L$^{-1}$) are the BSA concentrations in the feed solution and in the permeate at 20th min, respectively.

### 2.5. Batch adsorption test

A stock phosphate solution with a concentration of 1 g-P·L$^{-1}$ was prepared by dissolving KH$_2$PO$_4$ in DI water. The stock solution was diluted using DI water to prepare phosphate solutions for batch adsorption tests.

When the effect of pH was investigated, 50 ml phosphate solutions (1 mg-P·L$^{-1}$) with different pH were prepared. The pH value was adjusted by 1 mol·L$^{-1}$ HCl and 1 mol·L$^{-1}$ NaOH. The fabricated membranes were cut into small pieces (approximately 0.3 cm ×0.3 cm). 0.5 g dry membrane pieces were added into the phosphate solution. The mixture was shaken at 200 rpm at 25°C for 10 h. A similar procedure was also carried out to investigate the effect of co-existing anions (Cl$^-$, SO$_4^{2-}$, HCO$_3^-$) on phosphate removal except that the pH of the prepared solutions was not adjusted.

In the adsorption kinetics study, 0.5 g dry membrane pieces were added into 50 ml phosphate solutions with the phosphate concentrations of 1 mg-P·L$^{-1}$ and 50 mg-P·L$^{-1}$, respectively. No pH adjustment was conducted. The solution was shaken at 25°C and samples were collected at different time intervals.

In the adsorption isotherm study, 0.5 g dry membrane pieces were added into 50 ml solutions with different phosphate concentrations. The protocol was similar as that of pH effect study except that the solution pH was not adjusted.

In order to investigate the regeneration of the prepared Fe$_3$O$_4$/PSf membranes after phosphate adsorption, the used membrane pieces were immersed in a 0.01 mol·L$^{-1}$ NaOH solution for 2 h at 200 rpm, followed by washing with DI water. The regenerated membrane was then reused in the adsorption test.

### 2.6. Analytical

The crystal structure of Fe$_3$O$_4$ NPs was examined by X-ray diffraction analysis (XRD, D/MAX-2500, Rigaku). Their morphology was studied by transmission electron microscopy (TEM, H-7650, Hitachi). The particle size distribution of Fe$_3$O$_4$ NPs in NMP was analyzed by dynamic light scatter (DLS, Zetasizer NanoZS90, Malvern). The morphologies of both Fe$_3$O$_4$/PSf membrane surface and cross-section were observed using scanning electron microscopy (SEM, G2 pure, Phenom). The cross-sectional samples were obtained by fracturing in liquid nitrogen. All membrane samples were spur-coated with gold before SEM analysis. The water contact angles (CA) were measured using a contact angle goniometer (JC2000C, Powereach).

Membrane porosity was determined by the mass difference method. The prepared membrane was soaked in DI water until membrane pores were fully filled with water. Excess water attached on membrane surface was removed by filter paper before the wet weight ($W_w$, kg) was determined. The same membrane was then dried in a vacuum oven at 50°C for 24 h, and its dry weight ($W_d$, kg) was determined after cooling to room temperature. The membrane porosity ($P_r$, %) was calculated by Eq. (3)

$$P_r = \frac{W_w - W_d}{\rho_w \cdot S \cdot l} \times 100\% \tag{3}$$

where $\rho_w$ (kg·m$^{-3}$) is the density of pure water at 25°C; $S$ (m$^2$) is the area of membrane; $l$ (m) is the thickness of membrane which was determined using a digital micrometer.

Membrane meanpore size (nm) was calculated using Guerout-Elford-Ferry equation:

$$r_m = 5.37 \times 10^9 \times \sqrt{\frac{(2.9 - 1.75 P_r) \cdot \eta \cdot l \cdot J}{P_r \cdot \Delta P}} \tag{4}$$

where $J$ (L·m$^{-2}$·s$^{-1}$) is the pure water flux; $\eta$ (Pa·s) is the water viscosity; $\Delta P$ (Pa) is the transmembrane pressure.

BSA concentration was determined by its absorption at 280 nm using UV spectrophotometer (UV-2550, Shimadzu) [16]. Phosphate concentrations were determined by the Mo-Sb spectrophotometry [17]. Fe concentration in solution was determined by inductively coupled plasma-optical emission spectrometry (ICP-OES, Varian715-ES, Agilent).

## 3. Results and discussion

### 3.1. XRD

The Fe$_3$O$_4$ NPs were prepared by co-precipitation. The characteristic diffraction peaks (Fig. 1) were namely
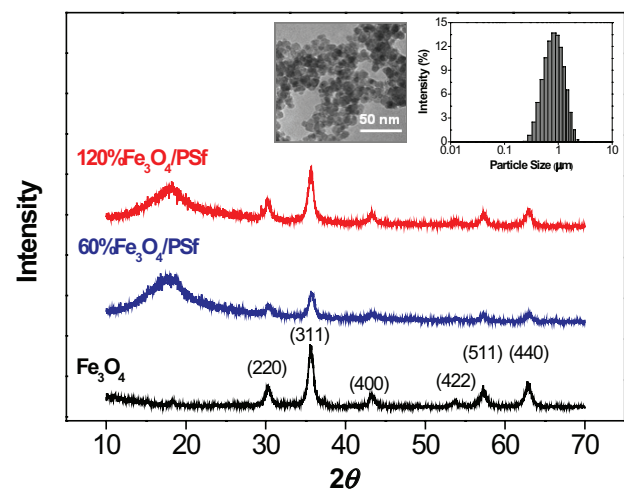


Fig. 1. XRD patterns of the prepared Fe$_3$O$_4$ nanoparticles and Fe$_3$O$_4$/PSf membrane. Inserts are TEM images of Fe$_3$O$_4$ nanoparticles and their particle size distribution in NMP solution, respectively.

18.3°, 30.1°, 35.5°, 43.1°, 53.5°, 57.0°, and 62.6°, which matched well with the spinel $Fe_3O_4$ according to the Joint Committee on Powder Diffraction Standards (JPCS) [18]. TEM analysis indicated that the individual $Fe_3O_4$ NPs were of regular spheres with diameters of around 10–15 nm, but stuck to each other to form bigger clusters. Similar aggregation phenomenon was also observed in previous literature [19]. Dynamic light scatter (DLS) reflected the hydro-dynamic size of particles, which was close to the aggregate size in solution. The apparent average size of the prepared $Fe_3O_4$ NPs in the NMP solution was around 800 nm, which also demonstrated the occurrence of the $Fe_3O_4$ NPs aggregation.

For 60% $Fe_3O_4$/PSf and 120% $Fe_3O_4$/PSf, the board peaks at 2θ = 17.7° in XRD patterns (Fig. 1) were the characteristic PSf peak [20]. Other prominent peaks observed were completely consistent with those of $Fe_3O_4$ NPs, indicating the successful incorporation of $Fe_3O_4$ NPs into the PSf matrix. The intensity of peaks assigned to the $Fe_3O_4$ NPs slightly decreased when the $Fe_3O_4$ NPs loading ratio was 60%. In the case of 120% $Fe_3O_4$/PSf, $Fe_3O_4$ NPs were better exposed in the MMMs, and therefore the corresponding peak intensity was more or less the same as that of the pristine $Fe_3O_4$ NPs.

## 3.2. SEM

SEM images of the prepared membranes are shown in Fig. 2. The pristine PSf membrane had an asymmetric structure with a dense skin layer on the top surface, and a finger-like structure in the upper layer followed by a macro-void structure in the sub-layer. Similar structure was typical for the flat sheet PSf membrane fabricated via NIPS [12]. $Fe_3O_4$ agglomerations were presented in both surface and cross section of the MMMs, and more and bigger aggregates were observed when the $Fe_3O_4$ loading increased to 120%. Morphological changes due to the $Fe_3O_4$ NPs addition were apparent in the membrane cross section. The finger-like structure of MMMs in the upper layer became much longer and wider compared to the pristine PSf membrane, while the macrovoid structure in the sub-layer markedly shrunk. In the case of 120% $Fe_3O_4$/PSf the clear boundary between the finger-like structure and the macrovoid structure disappeared, and uniform array channels with diameters around 16 µm appeared across the membrane thickness direction from top to bottom. Due to high affinity of $Fe_3O_4$ NPs towards water, $Fe_3O_4$ NPs addition in dope accelerated the exchange rate between solvent and water during the phase-inversion process. Therefore, opener finger-like structure without macrovoid was obtained.

## 3.3. Membrane properties

Membrane properties in terms of porosity, pore size, water contact angle, pure water flux, and BSA rejection are listed in Table 1.

The $Fe_3O_4$ NPs addition significantly increased the membrane porosity. This can be qualitatively predicted from the more porous structure of the sublayer due to the enhanced phase inversion kinetics as shown in Fig. 2. The porosity of the pristine PSf membrane was 54.2%, whereas for 60% $Fe_3O_4$/PSf it markedly increased to 76.4%. Further
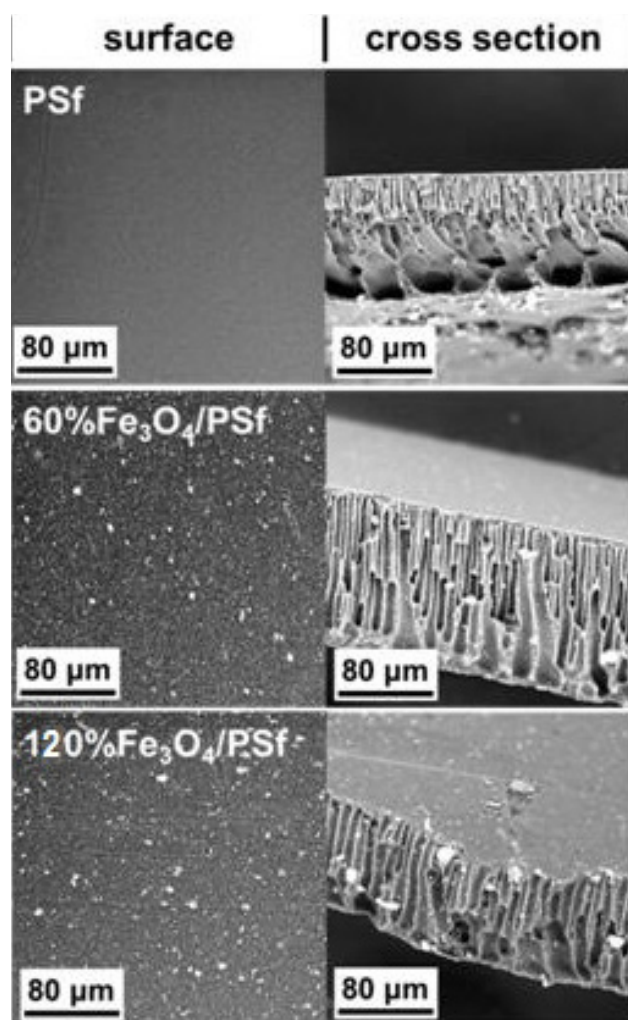


Fig. 2. SEM images of the prepared PSf and $Fe_3O_4$/PSf membranes.

increase in the $Fe_3O_4$ loading to 120% slightly enhanced the porosity to 80.1%. High porosity is generally a good sign for UF featured with high filtration flux [21].

The mean pore size of the pristine PSf membrane was 46.3 nm, which was qualified for UF membrane. The increase in $Fe_3O_4$ loading gradually decreased the pore size. This was probably because of the increase in the viscosity of the dope solution, which consequently suppressed the formation of large pores. In addition, the presence of $Fe_3O_4$ aggregates on membrane surface would blocked membrane pores and also resulted in the small pore size [22]. When $Fe_3O_4$ loading was 120%, the mean pore size decreased to 38.2 nm.

The water CA of the membranes slight decreased when the $Fe_3O_4$ loading was 60%. Therefore, the presence of $Fe_3O_4$ NPs increased the surface hydrophilicity of membrane. However, the membrane hydrophilicity of 120% $Fe_3O_4$/PSf was close to that of the pristine PSf membrane. $Fe_3O_4$ NPs were inherently hydrophilic, and the incorporation of a small amount of $Fe_3O_4$ can obtain membrane with higher hydrophilicity and less fouling potential [23]. Nevertheless,

Table 1
Properties of the prepared PSf and $Fe_3O_4$/PSf membranes

| Membrane | Porosity (%) | Mean pore size (nm) | Contact angle (°) | Pure water flux@0.1 MPa ($L \cdot m^{-2} \cdot h^{-1}$) | BSA rejection (%) |
|---|---|---|---|---|---|
| PSf | 54.2±1.2 | 46.3±0.6 | 81±0.2 | 330±8 | 95.4±1.2 |
| 60%$Fe_3O_4$/PSf | 76.4±1.7 | 43.8±0.2 | 75±0.2 | 455±8 | 86.5±2.7 |
| 120%$Fe_3O_4$/PSf | 80.1±1.2 | 38.2±0.1 | 81±0.1 | 438±7 | 94.4±1.4 |

the clear agglomeration on membrane surface observed at high $Fe_3O_4$ loading (120%) definitely increased the membrane surface roughness, which resulted in the decrease in membrane hydrophilicity.

Modified UF membrane by incorporating inorganic NPs is an effective tactic to enhance pure water flux (PWF). The heterogeneity between the addictives and the polymer changed the membrane structure with higher porosity [24]. The PWF@0.1 MPa of $Fe_3O_4$/PSf was around 450 $L \cdot m^{-2} \cdot h^{-1}$, which was 36% higher compared to that of the pristine PSf membrane. Even though the mean pore size decreased for $Fe_3O_4$/PSf, BSA rejection slight decreased instead, especially for 60%$Fe_3O_4$/PSf. The BSA molecular in water was less than 10 nm in size [25]. Therefore, the effective BSA rejection seemed incapable of being accomplished by clean pores via size exclusion. The adsorption of BSA due to its affinity with the polymer membrane was supposed to be the crucial reason for membrane fouling and consequently shrinking the membrane pores. As a result, the apparent BSA rejection was correlated with the membrane hydrophilicity. The enhanced hydrophilicity for 60%$Fe_3O_4$/PSf alleviated its adsorption of BSA, and therefore the rejection of BSA decreased to 86.5%. For 120%$Fe_3O_4$/PSf, the increase in hydrophobicity enhanced BSA rejection to 94.4%.

According to the results mentioned above, the $Fe_3O_4$/PSf membrane we prepared in this study well kept the properties of UF membrane and no defects were detected. The enhanced PWF as well as the decreased membrane pore size was favorable for the efficient and stable performance of UF for water treatment.

### 3.4. Filtration test

A 0.3 $g \cdot L^{-1}$ BSA solution was used as the feed solution to investigate the antifouling capability of the prepared $Fe_3O_4$/PSf membranes. BSA was a notorious foulant for polymer UF membranes [26]. As can be seen in Fig. 3, compared with PWF, the flux during the filtration of a BSA solution was almost completely lost in the case of pristine PSf membrane in 2 h. Severe fouling for PSf membrane due to the presence of BSA, a common surrogate for protein, was also reported in previous studies [27], which was mainly attributed to the strong hydrophobic affinity between protein and polymer. The high water CA of the PSf membrane as well as its high BSA rejection efficiency also supported the severe fouling phenomenon. For $Fe_3O_4$/PSf membranes, even though the membrane fouling was inevitable, the decline in flux was significantly alleviated. After 2 h filtration, the flux values were 210 $L \cdot m^{-2} \cdot h^{-1}$ and 170 $L \cdot m^{-2} \cdot h^{-1}$ for 60%$Fe_3O_4$/PSf and 120%$Fe_3O_4$/PSf, respectively. The flux of 120%$Fe_3O_4$/PSf exhibited a similar time profile as that of PSf membrane.
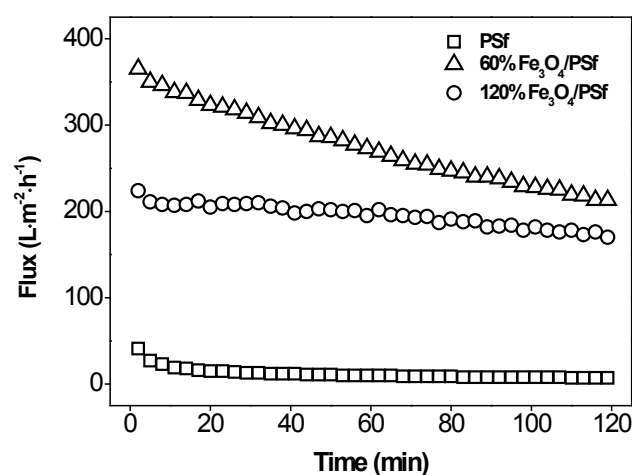


Fig. 3. Flux profile during the filtration of a BSA solution (0.3 $g \cdot L^{-1}$) at 0.1 MPa with PSf and $Fe_3O_4$/PSf membranes.

It dropped quickly at the very beginning and achieved a stable performance thereafter. This was a typical feature for the formation of gel fouling layer [28]. However, for 60%$Fe_3O_4$/PSf, the flux decreased gradually and no stable flux was obtained during the 2 h filtration. The significant difference was supposed to arise from the membrane hydrophilicity. Compared with 60%$Fe_3O_4$/PSf, the adsorption of BSA onto the pores of 120%$Fe_3O_4$/PSf was more serious due to its high hydrophobicity. The consequent decrease in membrane pore size accelerated the formation of gel layer, and the filtration became stable quickly. Overall, the incorporation of $Fe_3O_4$ NPs into PSf matrix produced excellent MMMs with improved performance in terms of high permeate flux and moderate fouling.

### 3.5. Phosphate adsorption

#### 3.5.1. Effect of pH

Fig. 4 shows the effect of initial pH on phosphate adsorption using the 120%$Fe_3O_4$/PSf membrane. The phosphate removal was rather stable when the solution pH varied from 2 to 8, indicating that the prepared MMMs worked well in acidic and neutral conditions. However, in the alkaline solution, the removal sharply deteriorated. Only 8.5% of phosphate was removed from the solution at pH 12. The adsorption of phosphate by $Fe_3O_4$ NPs was mainly based on the electrostatic attraction, which was strongly dependent on the dissociation of phosphate

and the charge of $Fe_3O_4$ NPs. As a polyprotic acid, phosphate mainly existed in the form of negatively charged species, namely $H_2PO_4^-$, $HPO_4^{2-}$, and $PO_4^{3-}$ at pH above 3. The isoelectric potential (IEP) of $Fe_3O_4$ NPs was close to 8 [29]. When the solution pH was above 8, $Fe_3O_4$ NPs were negatively charged. Therefore, the electrostatic repulsions between the phosphate and $Fe_3O_4$ NPs decreased the removal efficiency [30]. With the decrease of pH, the positive charge of $Fe_3O_4$ NPs became higher whereas $HPO_4^{2-}$ was gradually protonated and transferred to $H_2PO_4^-$. The attraction force was consequently stable, so was the removal of phosphate. When the solution pH decreased below 3, the percentage of non-ionized phosphoric acid increased. The electrostatic attraction was supposed to attenuate as a result. However, the removal efficiency seemed not to be affected even when the solution pH was 2. It was reported that the interaction with the hydroxyl sites at the surface of magnetite to form phosphate complexes also contributed to the phosphate removal, especially in an acidic condition [31,32]. In addition, it should be mentioned that $Fe_3O_4$ NPs dissolved at the strong acidic condition, and the release of $Fe^{3+}$ into the solution was detected in this study (Fig. 4). Therefore, the precipitation of iron phosphate was supposed to be another reason for the high phosphate removal at pH below 3. With respect to the membrane stability and the effluent quality, the prepared $Fe_3O_4$/PSf membrane was suggested to be used in pH range of 4–8, and in that case the Fe concentration released into the solution was less than 0.07 mg·$L^{-1}$.

### 3.5.2. Effect of co-existing anions

The effects of co-existing anions, namely $Cl^-$, $SO_4^{2-}$, and $HCO_3^-$, on phosphate removal were investigated using $120\%Fe_3O_4$/PSf (Fig. 5). The existence of $Cl^-$ and $SO_4^{2-}$ only slightly decreased the phosphate removal. The most serious decline was found in the presence $HCO_3^-$. When the $HCO_3^-$ concentration increased from zero to 250 mg·$L^{-1}$, the removal efficiency markedly decreased from 95% to 63%. It was attributed it to the pH increase arising from the $HCO_3^-$ dissociation. Bicarbonate is a pH buffering agent, and its presence in solution raised and buffered system pH above

neutral values [33]. In this study, the pH value of the test solution was above 9.2 in the presence of $HCO_3^-$, while that was neutral for other co-existing anions. Therefore, the impact of $HCO_3^-$ on phosphate uptake was much stronger compared to $Cl^-$ and $SO_4^{2-}$.

### 3.5.3. Adsorption kinetics

As shown in Fig. 6, adsorption tests with two different initial phosphate concentrations, namely 1 mg-P·$L^{-1}$ and 50 mg-P·$L^{-1}$, were conducted to study the kinetics of phosphate adsorption on the $Fe_3O_4$/PSf membranes. The uptake of phosphate by $Fe_3O_4$/PSf membranes was rather fast during the initial 1 h, followed by a slow adsorption process. The higher the initial phosphate concentration was, the shorter the slow adsorption process lasted. This was probably because high initial phosphate concentration provided strong mass transfer driving force for adsorption and accelerated the accomplishment of the equilibrium. It cost 3 h and 1 h to achieve the equilibrium for the initial phosphate concentrations of 1 mg-P·$L^{-1}$ and 50 mg-P·$L^{-1}$, respectively. The fast adsorption at the initial stage was favorable and necessary for the simultaneous removal of phosphate during the UF process. In addition, $Fe_3O_4$/PSf membrane with higher $Fe_3O_4$ loading showed higher phosphate uptake at equilibrium because it had more sites for adsorption.

The time profile of the adsorption was fitted by the kinetic models of pseudo-first order [Eq. (5)] and pseudo-second order [Eq. (6)], respectively.

$$\frac{dq_t}{dt} = k_1(q_e - q_t) \tag{5}$$

$$\frac{dq_t}{dt} = k_2(q_e - q_t)^2 \tag{6}$$

where $k_1$ ($min^{-1}$) and $k_2$ (g·mg-$P^{-1}$·$min^{-1}$) are rate constants for the pseudo-first order and the pseudo-second order models, respectively; $q_e$ (mg-P·$g^{-1}$) and $q_t$ (mg-P·$g^{-1}$) are the amount of phosphate adsorbed per unit mass of membrane at equilibrium and at time $t$ (min), respectively. The fitting results are listed in Table 2.
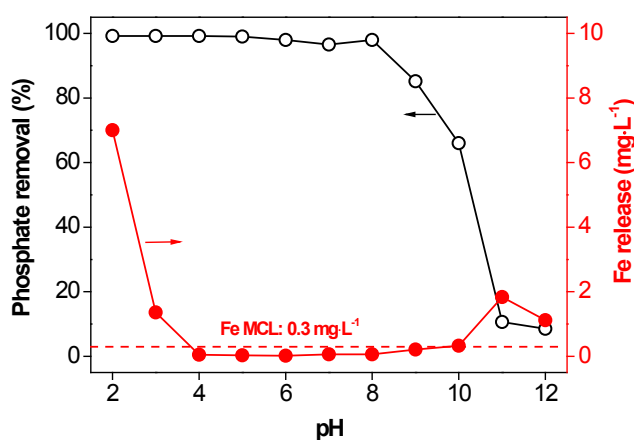


Fig. 4. Effect of pH on phosphate removal by the $120\%Fe_3O_4$/PSf membrane as well as on Fe leakage.
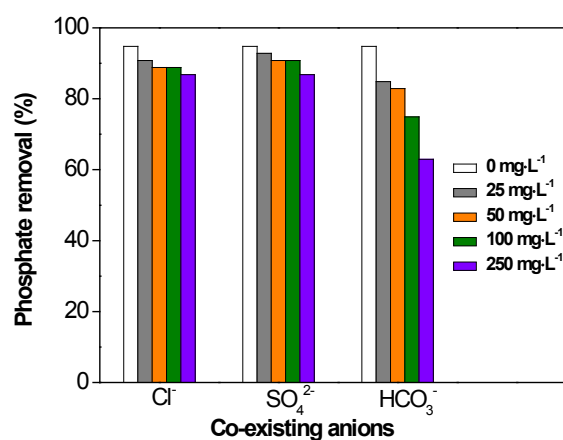


Fig. 5. Effect of co-existing anions on phosphate removal by the $120\%Fe_3O_4$/PSf membrane.

Both two kinetic models could depict the experimental results quite well (Fig. 6). According to the fitting results in Table 2, the correlation coefficients ($R^2$) calculated by pseudo-second order model were slightly higher than those calculated by pseudo-first order model, but all the $R^2$ values were higher than 0.96. The kinetics of Pb(II) removal using hydrous ferric oxide incorporated PSf membrane followed the pseudo-second order model, rather than the pseudo-first order model [12], while for arsenate adsorption by PSf membrane embedded with Zr-based nanoparticles both models
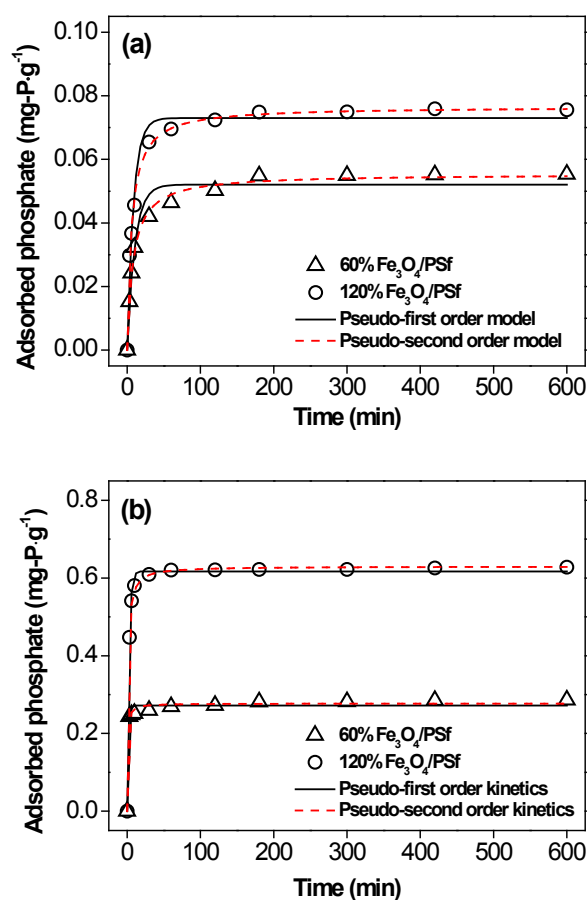


Fig. 6. Pseudo-first order and pseudo-second order of phosphate adsorption on the $Fe_3O_4$/PSf membranes with initial phosphate concentrations of 1 mg-P·L$^{-1}$ (a) and 50 mg-P·L$^{-1}$ (b) ($T$ = 25°C, initial pH = 7).

fitted the experimental data well [3]. In this study, the calculated $q_e$ value was similar to the experimental one for each test condition, and $Fe_3O_4$ NPs loading and initial phosphate concentration were positively correlated to the $q_e$ value.

Intra-particle diffusion model [Eq. (7)] was used to investigate the significance of intra-particle diffusion on the phosphate adsorption kinetics by $Fe_3O_4$/PSf membranes.

$$q_t = k_p t^{1/2} \qquad (7)$$

where $k_p$ is the intra-particle diffusion rate constant (mg-P·g$^{-1}$·min$^{-0.5}$). Generally speaking, adsorption process followed three consecutive steps, namely external diffusion, intra-particle diffusion, and adsorption [34]. The phosphate uptake between 30 and 180 min was employed for the intra-particle diffusion model analysis, and the obtained $k_p$ after linear fitting are listed in Table 2. Due to the enhancement of the driving force, the $k_p$ value significantly increased as the initial phosphate concentration increased from 1 mg-P·L$^{-1}$ to 50 mg-P·L$^{-1}$ [35]. The $k_p$ values for 60%$Fe_3O_4$/PSf membrane were higher than those for 120%$Fe_3O_4$/PSf membrane despite of the initial phosphate concentration, indicating the weaker significance of intra-particle diffusion for 120%$Fe_3O_4$/PSf membrane. This was probably because $Fe_3O_4$ agglomerations were mostly presented in the surface of the MMMs at high NPs loading. In all cases, the fitting lines did not pass through the origin. Therefore, intra-particle diffusion was not the rate-limiting step for the phosphate adsorption by $Fe_3O_4$/PSf membranes [36].

### 3.5.4. Adsorption isotherm

The uptake of phosphate onto the $Fe_3O_4$/PSf membranes increased with the phosphate concentration in solution, and more $Fe_3O_4$ loading benefited higher adsorption capacity (Fig. 8). The experimental data were analyzed using Langmuir [Eq. (8)] and Freundlich [Eq. (9)] isotherm models.

$$q_e = \frac{k_L q_m c_e}{1 + k_L c_e} \qquad (8)$$

$$q_e = k_F c_e^{1/n} \qquad (9)$$

where $q_m$ (mg-P·g$^{-1}$) is the maximum adsorption capacity; $q_e$ (mg-P·g$^{-1}$) and $c_e$ (mg-P·L$^{-1}$) are adsorption amount and aqueous concentration of phosphate at equilibrium, respectively; $k_L$ (L·mg-P$^{-1}$) is adsorption reaction constant; $k_F$ and $n$ are empirical constants.

Table 2
The fitting results of phosphate adsorption by $Fe_3O_4$/PSf membranes using kinetic models

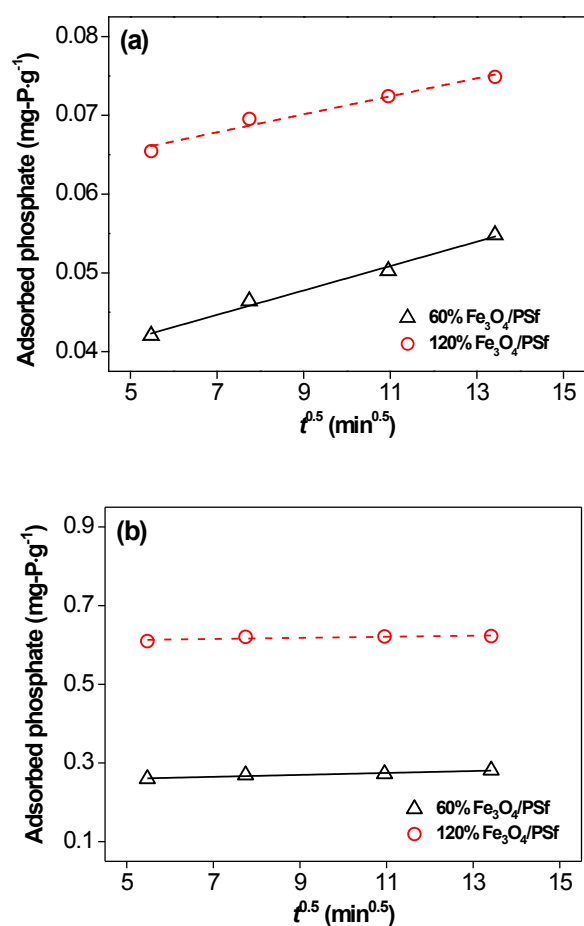| Initial P conc. (mg-P·L$^{-1}$) | Membrane | Pseudo-first order model | | | Pseudo-second order model | | | Intra-particle diffusion |
|---|---|---|---|---|---|---|---|---|
| | | $k_1$ (min$^{-1}$) | $q_e$ (mg-P·g$^{-1}$) | $R^2$ | $k_2$ (g·mg-P$^{-1}$·min$^{-1}$) | $q_e$ (mg-P·g$^{-1}$) | $R^2$ | $k_p$ (10$^{-3}$ mg-P·g$^{-1}$·min$^{-0.5}$) |
| 1 | 60%$Fe_3O_4$/PSf | 0.094 | 0.052 | 0.961 | 2.257 | 0.055 | 0.994 | 1.55 |
| | 120%$Fe_3O_4$/PSf | 0.115 | 0.073 | 0.973 | 2.216 | 0.077 | 0.995 | 1.14 |
| 50 | 60%$Fe_3O_4$/PSf | 0.703 | 0.272 | 0.975 | 6.656 | 0.277 | 0.989 | 2.47 |
| | 120%$Fe_3O_4$/PSf | 0.399 | 0.617 | 0.995 | 1.433 | 0.630 | 0.998 | 1.40 |

Fig. 7. Intra-particle diffusion of phosphate on $Fe_3O_4$/PSf membranes with initial phosphate concentrations of 1 mg-P·$L^{-1}$ (a) and 50 mg-P·$L^{-1}$(b) ($T$ = 25°C, initial pH = 7).



Fig. 8. Isotherms of phosphate adsorption on $Fe_3O_4$/PSf membranes ($T$ = 25°C, initial pH = 7).
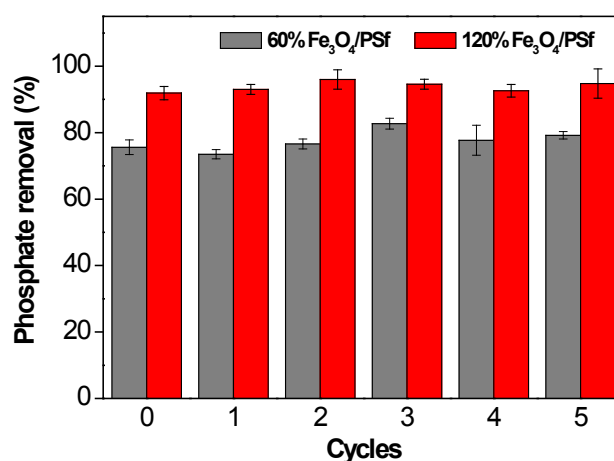


Fig. 9. Repeated uses of the regenerated $Fe_3O_4$/PSf membranes for phosphate removal.

The fitting results were overall reliable with the correlation coefficients ($R^2$) higher than 0.8. The Freundlich model fitted the experimental data slightly better than the Langmuir model did. The theoretical maximum adsorption capacity obtained by Langmuir isotherm was 0.440 mg-P·$g^{-1}$ and 0.684 mg-P·$g^{-1}$ for 60% $Fe_3O_4$/PSf and 120% $Fe_3O_4$/PSf, respectively. When the phosphate uptake was normalized to the $Fe_3O_4$ mass in membrane, the adsorbed phosphate per gram of $Fe_3O_4$ was around 1.2 mg-P·$g^{-1}$ for both membranes. This value was lower compared to previous studies on the phosphate removal using $Fe_3O_4$ NPs [6,29]. The inevitable coverage of the $Fe_3O_4$ NPs by PSf polymer in the prepared MMMs reduced the adsorption sites available for phosphate removal. Even though the phosphate adsorption capacity was partially lost, the use of $Fe_3O_4$/PSf membranes for phosphate removal was still attractive due to the elimination of the complex procedures for NPs recovery and recycle. In Freundlich isotherm, the value of $1/n$ can be used as an indicator for adsorption favorability [37]. It was generally believed that $1/n < 1$ implied a chemisorption on a relatively homogeneous surface while $1/n > 1$ implied a physical sorption [11]. The calculated $1/n$ values in this study were 0.384–0.503. Therefore, the adsorption of phosphate on $Fe_3O_4$/PSf membrane was based on chemical reac-
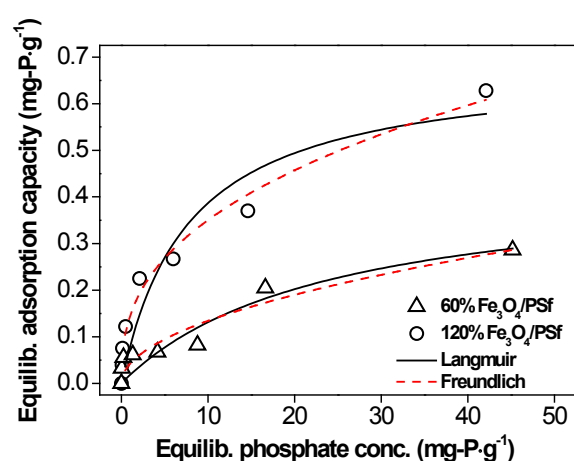
tions, which was consistent with the interaction between phosphate and $Fe_3O_4$ NPs [29].

### 3.5.5. Desorption

The removal of phosphate on $Fe_3O_4$/PSf membranes decreased dramatically in alkaline solution (pH > 12, Fig. 4). Therefore, a 0.01 mol·$L^{-1}$ NaOH solution was used to regenerate the exhausted membranes after phosphate adsorption. As shown in Fig. 9, after 5 adsorption/desorption cycles, the phosphate removal from the solution containing phosphate of 1 mg-P·$L^{-1}$ barely lost. The removal efficiency maintained around 78% and 94% for 60%$Fe_3O_4$/PSf and 120%$Fe_3O_4$/PSf, respectively. The outstanding desorption of phosphate from magnetite was also previously reported [29], whereas other iron oxides and hydroxides, such as goethite and akaganeite, demonstrated rather poor reusability [38]. Since alkaline solution was commonly used for chemical cleaning of the organic-fouled membranes, the regeneration of the

Table 3
The fitting results of phosphate adsorption by $Fe_3O_4$/PSf membranes using isotherm models

| Membrane | Langmuir | | | Freundlich | | |
|---|---|---|---|---|---|---|
| | $k_L$ (L·mg-P$^{-1}$) | $q_m$ (mg-P·g$^{-1}$) | $R^2$ | $k_F$ | $1/n$ | $R^2$ |
| 60%$Fe_3O_4$/PSf | 0.042 | 0.440 | 0.845 | 0.042 | 0.503 | 0.883 |
| 120%$Fe_3O_4$/PSf | 0.130 | 0.684 | 0.866 | 0.145 | 0.384 | 0.983 |

exhausted $Fe_3O_4$/PSf membrane after phosphate adsorption can be accomplished in the chemical cleaning procedure of the UF process.

## 4. Conclusions

In this study, MMMs with $Fe_3O_4$ NPs incorporation into PSf membrane were successfully prepared via NIPS method and used for phosphate removal from solution. XRD results confirmed the presence of $Fe_3O_4$ NPs in the PSf membrane matrix. The $Fe_3O_4$ NPs addition changed the membrane structure. With the increase in $Fe_3O_4$ NPs loading, the finger-like structure in membrane cross section became longer, and extended from top surface to bottom. Therefore, the membrane porosity increased significantly. The highest pure water flux was obtained at the $Fe_3O_4$ NPs loading of 60% due to its enhanced hydrophilicity. However, excessive $Fe_3O_4$ NPs loading resulted in the NPs agglomeration, and slightly decreased the membrane hydrophilicity. When a 0.3 g·L$^{-1}$ BSA solution was used as feed, the prepared composite membranes showed outstanding fouling resistance compared to the pristine PSf membrane with much higher permeate flux. The adsorption of phosphate by $Fe_3O_4$/PSf membrane was effective in a wide pH range from 4 to 8. The existence of Cl$^-$ and $SO_4^{2-}$ only slightly decreased the phosphate removal, but the most serious decline was found in the presence $HCO_3^-$. The kinetic tests indicated that it took 3 h and 1 h to achieve the adsorption equilibrium at the initial phosphate concentrations of 1 mg-P·L$^{-1}$ and 50 mg-P·L$^{-1}$, respectively. The time profile of phosphate uptake could be well depicted by both pseudo-first order and pseudo-second order models, and the intra-particle diffusion was not the rate-limiting step for the whole adsorption process. The Langmuir isotherms demonstrated that the maximum phosphate adsorption capacities were 0.440 mg·g$^{-1}$ and 0.684 mg·g$^{-1}$ for 60%$Fe_3O_4$/PSf and 120%$Fe_3O_4$/PSf, respectively. In addition, a 0.01 mol·L$^{-1}$ NaOH solution could effectively desorb the phosphate adsorbed by $Fe_3O_4$/PSf membrane and recover its adsorption capability. The proposed $Fe_3O_4$/PSf membrane possessed dual functions and had the potential to accomplish phosphate removal during the conventional UF process.

## References

[1] B.Q. Qin, G. Gao, G.W. Zhu, Y.L. Zhang, Y.Z. Song, Lake eutrophication and its ecosystem response, Chinese Sci. Bull., 58 (2013) 961–970.
[2] W. Huang, Y. Zhang, D. Li, Adsorptive removal of phosphate from water using mesoporous materials: A review, J. Environ. Manage., 193 (2017) 470–482.
[3] J. He, T. Matsuura, J.P. Chen, A novel Zr-based nanoparticle-embedded PSF blend hollow fiber membrane for treatment of arsenate contaminated water: Material development, adsorption and filtration studies, and characterization, J. Membr. Sci., 452 (2014) 433–445.
[4] J.A. Rentz, I.P. Turner, J.L. Ullman, Removal of phosphorus from solution using biogenic iron oxides, Water. Res., 43 (2009) 2029–2035.
[5] I.D. Vicente, A. Merino-Martos, L. Cruz-Pizarro, J.D. Vicente, On the use of magnetic nano and microparticles for lake restoration, J. Hazard. Mater., 181 (2010) 375–381.
[6] Y.J. Tu, C.F. You, C.K. Chang, M.H. Chen, Application of magnetic nano-particles for phosphorus removal/recovery in aqueous solution, J. Taiwan. Inst. Chem. E., 46 (2015) 148–154.
[7] A. Afkhami, M. Sabertehrani, H. Bagheri, Simultaneous removal of heavy-metal ions in wastewater samples using nano-alumina modified with 2,4-dinitrophenylhydrazine, J. Hazard. Mater., 181 (2010) 836–844.
[8] S. Moharami, M. Jalali, Effect of $TiO_2$, $Al_2O_3$, and $Fe_3O_4$ nanoparticles on phosphorus removal from aqueous solution, Environ. Prog. Sustain., 33 (2015) 1209–1219.
[9] L.G. Yan, K. Yang, R.R. Shan, T. Yan, J. Wei, Kinetic, isotherm and thermodynamic investigations of phosphate adsorption onto core-shell $Fe_3O_4$@LDHs composites with easy magnetic separation assistance, J. Colloid Interf. Sci., 448 (2015) 508–516.
[10] J. Liu, Q. Zhou, J. Chen, L. Zhang, N. Chang, Phosphate adsorption on hydroxyl-iron-lanthanum doped activated carbon fiber, Chem. Eng. J., 215–216 (2013) 859–867.
[11] P. Daraei, S.S. Madaeni, N. Ghaemi, E. Salehi, M.A. Khadivi, Novel polyethersulfone nanocomposite membrane prepared by PANI/$Fe_3O_4$ nanoparticles with enhanced performance for Cu(II) removal from water, J. Membr. Sci., 415–416 (2012) 250–259.
[12] N. Abdullah, R.J. Gohari, N. Yusof, A.F. Ismail, J. Juhana, Polysulfone/hydrous ferric oxide ultrafiltration mixed matrix membrane: Preparation, characterization and its adsorptive removal of lead (II) from aqueous solution, Chem. Eng. J., 289 (2016) 28–37.
[13] T.S. Chung, L.Y. Jiang, Y. Li, S. Kulprathipanja, Mixed matrix membranes (MMMs) comprising organic polymers with dispersed inorganic fillers for gas separation, Prog. Polym. Sci., 32 (2007) 483–507.
[14] Y.M. Zheng, S.W. Zou, K.G.N. Nanayakkara, T. Matsuura, J.P. Chen, Adsorptive removal of arsenic from aqueous solution by a PVDF/zirconia blend flat sheet membrane, J. Membr. Sci., 374 (2011) 1–11.
[15] N. Ghaemi, S.S. Madaeni, P. Daraei, H. Rajabi, S. Zinadini, Polyethersulfone membrane enhanced with iron oxide nanoparticles for copper removal from water: Application of new functionalized $Fe_3O_4$ nanoparticles, Chem. Eng. J., 263 (2015) 101–112.
[16] Z. Fan, Z. Wang, M. Duan, J. Wang, S. Wang, Preparation and characterization ofpolyaniline/polysulfone nanocomposite ultrafiltration membrane, J. Membr. Sci., 310 (2008) 402–408.
[17] L.M. Ma, D. Rena, M. Zhang, J.F. Zhao, M. Com, Phosphorus fractions and soil release in alternately waterlogged and drained environments at the water-fluctuation-zone of the Three Gorges Reservoir, J. Food. Agric. Environ., 8 (2010) 1329–1335.

[18] X. Liang, X. Wang, J. Zhuang, Y. Chen, D. Wang, Synthesis of nearly monodisperse iron oxide and oxyhydroxide nanocrystals, Adv. Funct. Mater., 16 (2006) 1805–1813.

[19] O.U. Rahman, S.C. Mohapatra, S. Ahmad, $Fe_3O_4$ inverse spinal super paramagnetic nanoparticles, Mater. Chem. Phys., 132 (2012) 196–202.

[20] E. Shokri, R. Yegani, B. Pourabbas, N. Kazemian, Preparation and characterization of polysulfone/organoclay adsorptive nanocomposite membrane for arsenic removal from contaminated water, Appl. Clay Sci., 132–133 (2016) 611–620.

[21] H. Bessbouss, J.F. Verchère, L. Lebrun, Increase in permeate flux by porosity enhancement of a sorptive UF membrane designed for the removal of mercury(II), J. Membr. Sci., 364 (2010) 167–176.

[22] E. Demirel, B. Zhang, M. Papakyriakou, S. Xia, Y. Chen, $Fe_2O_3$ nanocomposite PVC membrane with enhanced properties and separation performance, J. Membr. Sci., 529 (2017) 170–184.

[23] S. Zinadini, A.A. Zinatizadeh, M. Rahimi, V. Vatanpour, H. Zangeneh, Novel high flux antifouling nanofiltration membranes for dye removal containing carboxymethyl chitosan coated $Fe_3O_4$ nanoparticles, Desalination, 349 (2014) 145–154.

[24] J.M. Arsuaga, A. Sotto, G.D. Rosario, A. Martínez, S. Molina, Influence of the type, size, and distribution of metal oxide particles on the properties of nanocomposite ultrafiltration membranes, J. Membr. Sci., 428 (2013) 131–141.

[25] S. Wang, K. Chen, L. Li, X. Guo, Binding between proteins and cationic spherical polyelectrolyte brushes: Effect of pH, ionic strength, and stoichiometry, Biomacromolecules, 14 (2013) 818–827.

[26] Z. Gao, L. Wang, R. Miao, N. Mi, S.S. Li, M. Zhu, Effect of pH on UF membrane fouling of organic foulant (BSA), J. Environ. Sci.-China, 35 (2015) 3640–3645.

[27] B. Ma, C. Hu, X. Wang, Y. Xie, W.A. Jefferson, Effect of aluminum speciation on ultrafiltration membrane fouling by low dose aluminum coagulation with bovine serum albumin (BSA), J. Membr. Sci., 492 (2015) 88–94.

[28] H. Hong, M. Zhang, Y. He, J. Chen, H. Lin, Fouling mechanisms of gel layer in a submerged membrane bioreactor, Bioresource, Technol., 166 (2014) 295–302.

[29] T.J. Daou, S. Begin-Colin, J.M. Grenèche, F. Thomas, A. Derory, Phosphate adsorption properties of magnetite-based nanoparticles, Chem. Mater., 19 (2007) 4494–4505.

[30] H. Shen, Z. Wang, A. Zhou, J. Chen, M. Hu, X. Dong, Adsorption of phosphate onto amine functionalized nano-sized magnetic polymer adsorbents: mechanism and magnetic effects, RSC Adv., 5 (2015) 22080–2209.

[31] J. Antelo, M. Avena, S. Fiol, R López, F. Arce, Effects of pH and ionic strength on the adsorption of phosphate and arsenate at the goethite-water interface, J. Colloid. Interf. Sci., 285 (2005) 476–486.

[32] A. Zach-Maor, R. Semiat, H. Shemer, Adsorption–desorption mechanism of phosphate by immobilized nano-sized magnetite layer: Interface and bulk interactions, J. Colloid. Interf. Sci., 363 (2011) 608–614.

[33] M.S. Onyango, Y. Kojima, O. Aoyi, E.C. Bernardo, H. Matsuda, Adsorption equilibrium modeling and solution chemistry dependence of fluoride removal from water by trivalent-cation-exchanged zeolite F-9, J. Colloid. Interf. Sci., 279 (2004) 341–350.

[34] A. Ozer, G. Dursun, Removal of methylene blue from aqueous solution by dehydrated wheat bran carbon, J. Hazard. Mater., 146 (2007) 262–269.

[35] Y. Xie, S. Li, G. Liu, J. Wang, K. Wu, Equilibrium, kinetic and thermodynamic studies on perchlorate adsorption by cross-linked quaternary chitosan, Chem. Eng. J., 192 (2012) 269–275.

[36] S. Chatterjee, S.H. Woo, The removal of nitrate from aqueous solutions by chitosan hydrogel beads, J. Hazard. Mater., 164 (2009) 1012–1018.

[37] J. Lalley, C. Han, X. Li, D.D. Dionysiou, M.N. Nadagouda, Phosphate adsorption using modified iron oxide-based sorbents in lake water: Kinetics, equilibrium, and column tests, Chem. Eng. J., 284 (2016) 1386–1396.

[38] R. Chitrakar, S. Tezuka, A. Sonoda, K. Sakane, K. Ooi, Phosphate adsorption on synthetic goethite and akaganeite, J. Colloid. Interf. Sci., 298 (2006) 602–608.